ADVANCES IN NUCLEAR SCIENCE AND APPLICATIONS

Volume 1, No. 2 (2025), P. 80-90

Two-body mechanisms in light-ion reactions with ^{9}Be

S.M. Lukyanov, A.V. Shakhov

Joint Institute for Nuclear Research, Dubna, Russia

e-mail: lukyan@jinr.ru

DOI: 10.63907/ansa.v1i2.36
Received: 28 May 2025

Abstract

Few-nucleon transfer reactions induced by light projectiles (d, ^{3}He, and ^{4}He) on the weakly bound nucleus ^{9}Be were investigated at incident energies of 26–35 MeV. Inclusive energy spectra and angular distributions were measured for outgoing fragments (p, d, t, ^{4}He, ^{7}Li, and ^{7}Be), allowing reconstruction of excitation energy spectra for the complementary residual nuclei. The observed spectral shapes are consistent with discrete level populations in both bound and unbound systems, supporting a dominant two-body reaction mechanism.

Special attention was given to channels involving short-lived unbound nuclei (^{5}He, ^{5}Li, and ^{8}Be). The extracted energy peaks and widths indicate population of these systems predominantly in their ground states. Comparisons with phase-space models and kinematic simulations exclude a statistical three-body decay scenario and confirm the formation of binary final states.

A time-scale analysis based on resonance widths yields equilibration times shorter than 10^{-22} s, suggesting that energy sharing occurs rapidly in these reactions. These findings support a cluster-transfer picture in which preformed configurations, such as ^{5}He and α clusters, are coherently transferred. The results provide new constraints on reaction dynamics and cluster structure in light nuclei.

Keywords: cluster transfer; two-body mechanism; unbound nuclei; excitation spectra; equilibration timescale

1 Introduction

Nuclear reactions, in which two incoming "particles" interact to form one or more products distinct from the initial participants, are fundamental processes in nuclear physics. Such a reaction must involve the transformation of at least one particle into another. A projectile interacts with one or more nucleons in the target nucleus, transferring energy or modifying the nucleonic composition (via transfer or capture) in a fast event with characteristic timescale $10^{-22} < \tau < 10^{-20}$ s [1]. When a low-energy projectile (up to 20 MeV/nucleon) enters the nuclear interaction zone, it may scatter or initiate a series of collisions with target nucleons [1]. These collisions may lead to the emission of particles and result in pre-equilibrium products, including the residual nucleus and any emitted fragments.

At low incident energies, the interaction often proceeds via full energy sharing among nucleons of the target and the projectile without prompt emission, forming a compound nucleus with $A + x$ nucleons, where x is the number brought in by the projectile. The excitation energy of this highly unstable system equals the kinetic energy of the projectile (in the center-of-mass system) plus its binding energy in the new configuration. Light weakly bound nuclei such as the deuteron, ^{6}He , ^{6,7}Li , and to a lesser extent ^{3}H and ^{3}He , are known to fragment easily in such reactions [2]. Theoretical approaches such as the Distorted-Wave Born Approximation (DWBA) and the Continuum-Discretized Coupled Channels (CDCC) method were developed decades ago, but their applications have gained prominence in recent years.

In this study, the weakly bound nucleus ^{9}Be was selected as a target to explore potential multi-body decay channels in the final state [1]. The ^{9}Be system is particularly notable due to its low one-neutron separation energy ($S_{1n} = 1.7$ MeV), which is even smaller than that of the unbound ^{6}He nucleus. Additionally, ^{9}Be exhibits a Borromean structure, often modeled as a three-body configuration α+α+n , in which none of the binary subsystems are bound [3]. This structure allows for several possible decay pathways, including:

- $^{9}\text{Be} \rightarrow^{8}\text{Be} + n \rightarrow \alpha + \alpha + n$
- $^{9}\text{Be} \rightarrow^{5}\text{He} + \alpha \rightarrow \alpha + \alpha + n$
- $^{9}\text{Be} \rightarrow \alpha + \alpha + n$

These breakup scenarios are closely tied to cluster transfer mechanisms [4]. Experimental studies have quantified the relative yields of the $n + {}^{8}\text{Be}_{\text{g.s.},2+}$ and $^{5}\text{He} + \alpha$ channels and shown that higher-lying excited states ($E^* > 4$ MeV) of ^{9}Be predominantly decay via $^{5}\text{He}_{\text{g.s.}}$. This highlights the importance of investigating both the internal cluster configurations ($^{8}\text{Be} + n$, $^{5}\text{He} + \alpha$) and their roles in nuclear reactions.

A central issue in the study of cluster transfer reactions is whether multi-nucleon transfers proceed via a direct (one-step) mechanism or through sequential (multi-step) processes. This question is particularly pertinent for loosely bound systems, such as the dineutron ($2n$) or ^{5}He clusters, where the spatial correlations between nucleons can significantly influence the transfer dynamics. Theoretical descriptions have been formulated for direct ^{5}He transfer mechanisms in reactions like $^{9}\text{Be}(p,{}^{6}\text{Li})$ [5], $^{16}\text{O}(p,{}^{6}\text{Li})^{11}\text{C}$ [6] and $^{11}\text{B}(p,{}^{6}\text{Li})^{6}\text{Li}$ [6].

Due to its Borromean structure, ^{9}Be is often modeled as a two-body cluster system, with configurations such as $^{8}\mathrm{Be} + n$ or $^{5}\mathrm{He} + \alpha$. The breakup via the $^{8}\mathrm{Be}_{\mathrm{g.s.}}$ channel is well established [7, 8, 9, 10], but the decay via the $^{8}\mathrm{Be}(2^{+})$ or $^{5}\mathrm{He}_{\mathrm{g.s.}}$ channels remains ambiguous. Theoretical studies offer differing conclusions: Grigorenko [11] suggested these broad intermediate resonances contribute little to the ($\alpha\alpha n$) reaction rate, while Buchmann [12] argued for a significant role of the $^{5}\mathrm{He}_{\mathrm{g.s.}}$ channel in stellar environments.

Soić et al. [13] provided the first direct experimental evidence that excited states of ^{9}Be around 6.5 and 11.3 MeV decay into the $\alpha + {}^{5}$He channel. Charity et al. [14] explored isobaric analog states in ^{9}B and found a dominant $\alpha + {}^{5}$Li decay, implying mirror decay via $\alpha + {}^{5}$He in ^{9}Be.

However, this interpretation is debated. Papka et al. [10] reported that the 2.429 MeV state decays primarily by neutron emission to $^{8}\mathrm{Be}(2^{+})$ rather than via $\alpha + {}^{5}$He. Most studies agree on a branching ratio of $\sim 7\%$ to $^{8}\mathrm{Be}_{\mathrm{g.s.}} + n$ [9], but division of the remaining strength between $^{8}\mathrm{Be}(2^{+})$ and $^{5}\mathrm{He} + \alpha$ remains unresolved. Nyman et al. [15] suggested a ratio of about 2:1 in favor of the former.

These findings point to the necessity of measuring branching ratios for low-lying states in ^{9}Be. The current experiment aims to quantify the relative importance of the $^{5}\mathrm{He} + \alpha$ and $n + {}^{8}$Be channels using inclusive measurements. Though lacking full event reconstruction, such measurements still provide insight into cluster structures. For instance, our earlier work [16] found large deformation parameters, interpreted as evidence for cluster structure, but could not resolve whether the dominant configuration was $\alpha + \alpha + n$ or $\alpha + {}^{5}$He.

We also investigate whether a cluster such as an α or ^{5}He is transferred as a coherent unit. D è traz et al. [4, 17] suggested that multi-particle–multi-hole states may form at relatively low excitation energies in light nuclei, enabling the transfer of preformed clusters. Understanding whether such transfer involves a single dominant internal configuration or a mix of competing ones is a core objective of this study.

A secondary goal is to revisit the $^{9}\mathrm{Be} + {}^{3}$He reaction and seek experimental evidence of cluster substructures within the products, offering further insight into the clustering nature of this Borromean nucleus.

2 Experimental Setup

Experiments employing accelerated ^{3}He and ^{4}He ion beams were carried out at the Jyväskylä Accelerator Laboratory (Finland) and the Nuclear Physics Institute in Řež (Czech Republic). The beam energies were 30MeV for ^{3}He and 26MeV for ^{4}He, with an average current of approximately 10nA. Comprehensive descriptions of the experimental setup and preliminary results are available in Refs.[16, 18, 19].

Targets consisted of self-supporting beryllium metal foils with a thickness of 12 μm. Reaction products were detected using arrays of three-stage silicon detector telescopes, configured as $\Delta E_0 - \Delta E - E_r$. These detectors measured energy losses (ΔE_0, ΔE) and residual energy (E_r), enabling particle identification across a broad Z range. The respective thicknesses of the detectors were 10 μm, 100 μm, and 3500 μm, providing sufficient resolution to distinguish charged particles from hydrogen up to beryllium isotopes ($Z = 1$–4).

Two-dimensional yield distributions as functions of ΔE and E_r for the $^{4}\mathrm{He}+{}^{9}$Be and $^{3}\mathrm{He} + {}^{9}$Be reactions confirmed that the detector systems facilitated clear

identification of reaction products. This included channels corresponding to elastic and inelastic scattering, as well as nucleon transfer processes. Isotopic and elemental discrimination was achieved via combined Z and A identification, while the total kinetic energy of the detected products was reconstructed from the sum of the calibrated energy deposits in each stage.

3 The ^{4}He(26 MeV) + ^{9}Be Reaction

Figure 1 presents the contour plot of reaction product yields as a function of the specific energy loss ΔE and the residual energy E_r, measured using the $\Delta E - E$ telescope for the $^4\mathrm{He} + {}^9\mathrm{Be}$ reaction [16]. The plot demonstrates well-separated loci corresponding to light charged particles [protons (p), deuterons (d), and tritons (t)] as well as heavier boron isotopes. These ridges are distinguished by their characteristic energy loss signatures, consistent with the expected behavior from the Bethe-Bloch formalism. The detector system shows excellent resolution and particle identification capabilities, allowing for clear separation of different isotopes across a broad energy range.

In addition to the hydrogen isotopes, the ground states of the residual nuclei ^{10}B, ^{11}B, and ^{12}B are prominently identified as isolated clusters at higher total energies. These peaks correspond to binary breakup channels where the detected light ejectile is emitted in coincidence with a bound boron fragment. The presence of these discrete peaks suggests that the reaction proceeds predominantly through direct two-body mechanisms, rather than through compound nucleus formation and subsequent statistical decay.

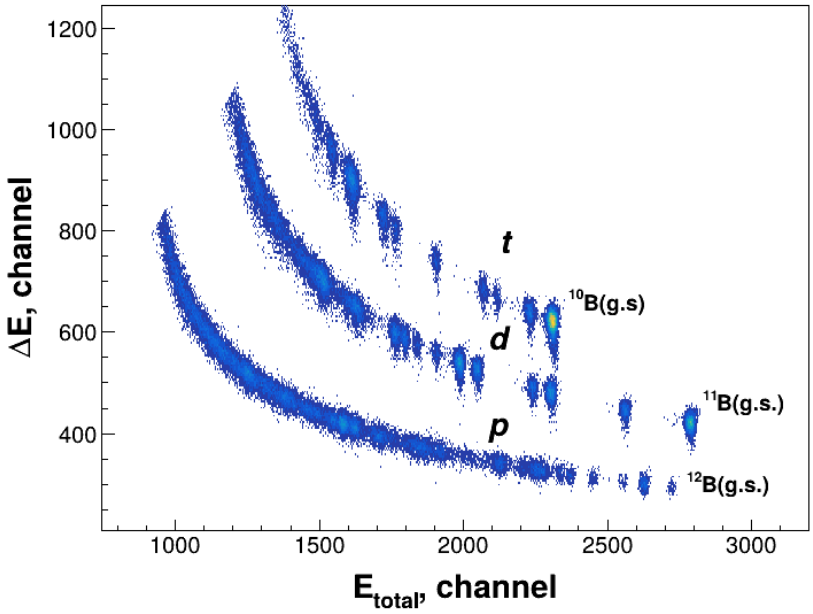

Figure 1: Contour plot of product yields as a function of ΔE and E_r measured using the $\Delta E - E$ telescope for the $^4\mathrm{He} + {}^9\mathrm{Be}$.

Excitation energy spectra of ^{10}B, ^{11}B, and ^{12}B, measured in the ^{4}He (26 MeV)+

^{9}Be reaction, are presented in Figure 2. These spectra were reconstructed from the measured energy distributions of emitted protons, deuterons, and tritons.

The observed distributions closely follow the excitation patterns of their respective complementary residual nuclei: ^{12}B , ^{11}B , and ^{10}B . The clear energy correlation between the light particles and the discrete states of the residual fragments strongly supports the dominance of binary reaction channels. This behavior is a characteristic signature of a kinematically correlated two-body process, in which the available energy is shared between the emitted light ejectile and the residual nucleus.

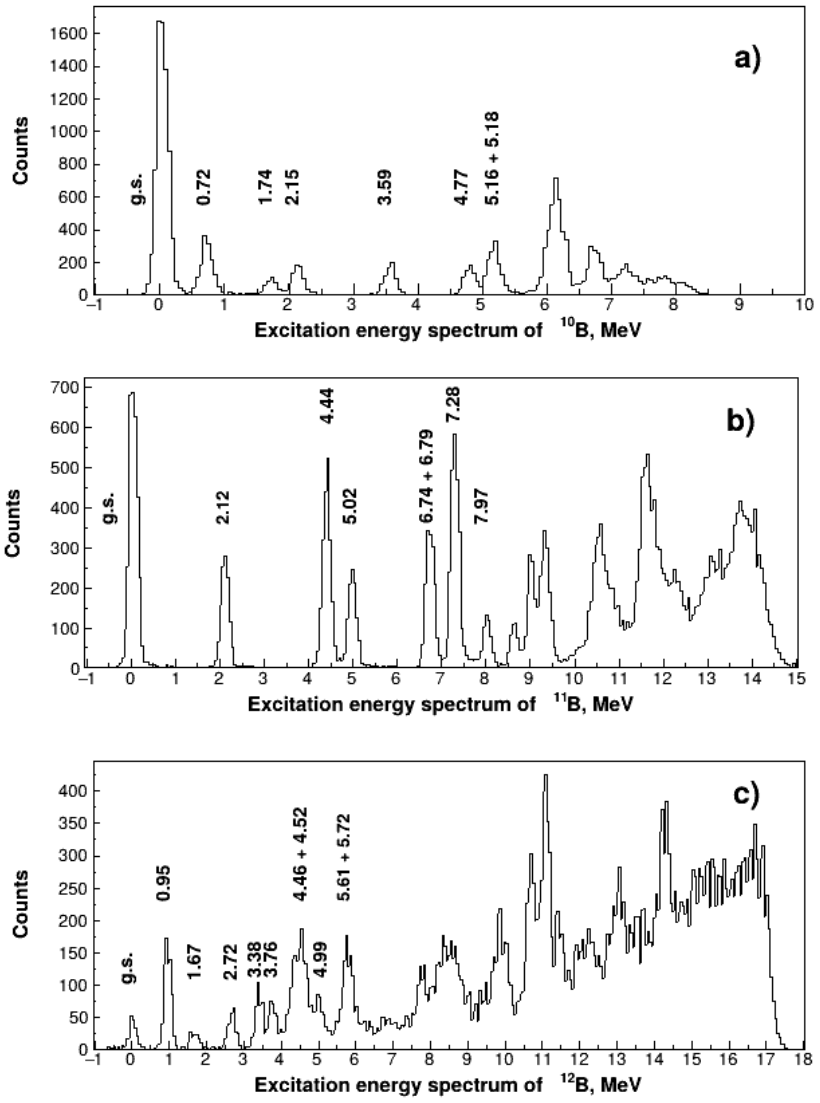

Figure 2: Exitation energy spectra of ^{10}B (a), ^{11}B (b), and ^{12}B (c) measured in the ^{4}He(26 MeV) + ^{9}Be reaction.

The excitation energy spectra exhibit well-resolved, narrow peaks corresponding to discrete states in the boron isotopes. The sharpness of these structures indicates excellent energy resolution of the detection system, enabling reliable separation of neighboring excited states. Based on the full width at half maximum (FWHM) of the lowest excited levels, the typical resolution is estimated to be around 300 keV. This level of resolution is sufficient to resolve individual low-lying nuclear levels and

confirms the suitability of the experimental setup for detailed spectroscopic studies of reaction mechanisms and nuclear structure.

The narrow widths and sharp onsets of the observed peaks effectively exclude significant contributions from statistical emission mechanisms. Instead, the data suggest that resonant processes or direct cluster-transfer reactions are likely involved in the reaction dynamics. In particular, the selective population of specific states in the boron isotopes implies sensitivity to nuclear structure effects, such as underlying cluster configurations in the entrance or exit channels.

Taken together, the ΔE - E particle identification and the reconstructed excitation spectra provide compelling evidence for direct reaction mechanisms, indicating that compound nucleus formation is not necessary to explain the observed energy distributions in these channels.

4 The ^{3}He(30 MeV) + ^{9}Be Reaction

In the previously discussed ^{4}He (26 MeV)+^{9}Be reaction, the complementary residual products are either bound boron isotopes ^{10,11}B or the strongly bound ^{12}B nucleus. In contrast, the use of a ^{3}He beam allows us to explore reaction channels in which the complementary nuclear systems are unbound. This enables access to a different regime of nuclear breakup dynamics, cluster structure, and resonance behavior.

In particular, we investigate the following reactions:

$$^{9}\mathrm{Be}(^{3}\mathrm{He},^{4}\mathrm{He})^{8}\mathrm{Be}, \quad ^{9}\mathrm{Be}(^{3}\mathrm{He},^{7}\mathrm{Be})^{5}\mathrm{He}, \quad ^{9}\mathrm{Be}(^{3}\mathrm{He},^{7}\mathrm{Li})^{5}\mathrm{Li}.$$

Figure 3 presents contour plots of the reaction yield distributions for the ^{3}He+^{9}Be reaction, displayed as functions of energy loss and residual energy ($\Delta E - E_r$, panel a) and of two successive energy losses ($\Delta E_0 - \Delta E$, panel b) [18, 19]. These plots provide a clear representation of the detector system's ability to identify reaction products and offer insight into the population and decay of unbound intermediate nuclear configurations.

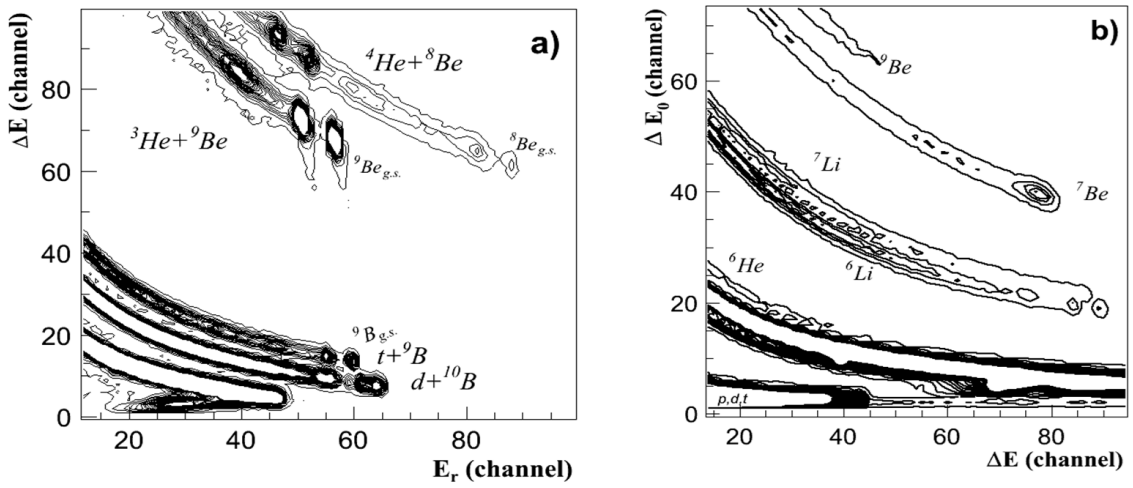

Figure 3: Contour plots of product yields as functions of $\Delta E - E_r$ (a) and $\Delta E_0 - \Delta E$ (b), obtained for the ^{3}He +^{9} Be reaction [18, 19].

Energy spectra of ^{4}He , ^{7}Be , and ^{7}Li reaction products, measured at a laboratory angle of $\theta_{\mathrm{lab}} = 18^{\circ}$, are presented in Figure 4. These spectra correspond to

reaction channels that populate unbound complementary nuclei: ^{8}Be , ^{5}He , and ^{5}Li , respectively [18, 19]. The observed structures reflect the underlying decay properties and kinematics of these unbound systems and provide insight into the cluster configurations and resonance behavior of the involved states.

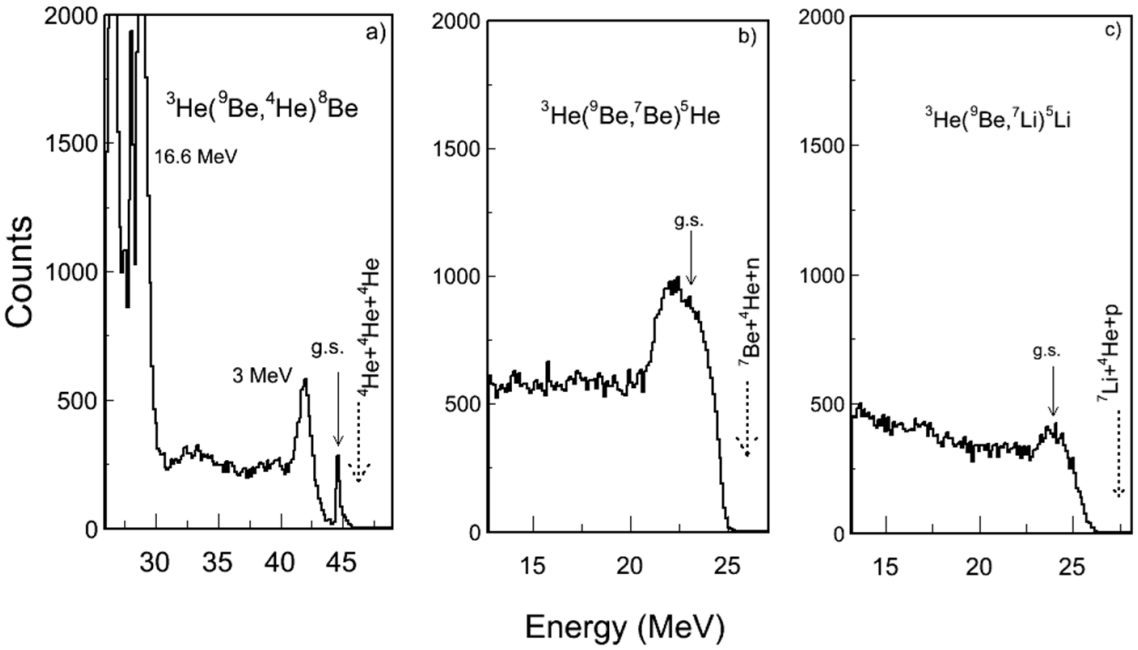

Figure 4: Energy spectra of ^{4}He (a), ^{7}Be (b), and ^{7}Li (c) fragments measured at $\theta_{\text{lab}} = 18^{\circ}$ for the ^{3}He +^{9} Be reaction . Solid arrows mark observed peaks corresponding to two-body final states in the ground state. Dashed arrows indicate expected thresholds for genuine three-body decays [18, 19].

Figure 4 illustrates the energy spectra of ^{4}He , ^{7}Be , and ^{7}Li fragments observed at $\theta_{\text{lab}} = 18^{\circ}$, providing insights into the excitation modes of the associated unbound residual systems. The structure of these spectra points toward a two-body reaction mechanism. To examine this interpretation, we carried out kinematic modeling assuming a three-body final state, in which all products emerge directly from the primary interaction.

Energy distributions of the decay fragments originating from short-lived unbound nuclei such as ^{8}Be , ^{5}He , and ^{5}Li were computed using the NRV database [2]. These nuclei decay into $^{4}\text{He} + {}^{4}\text{He}$, $^{4}\text{He} + n$, and $^{4}\text{He} + p$, respectively. The resulting distributions exhibit sharp onsets at threshold energies, marked by dashed arrows in Figure 4, and serve as a benchmark for distinguishing statistical from resonant decays. In a scenario dominated by phase-space kinematics, one would expect broad, featureless spectra without distinct peaks.

Contrary to these expectations, the measured spectra reveal well-defined peaks (highlighted by solid arrows), corresponding to resonant states of the unbound nuclei. For instance, in the $^{9}\text{Be}(^{3}\text{He}, ^{7}\text{Be})^{5}\text{He}$ reaction, a prominent ^{7}Be peak near 25MeV indicates the population of the ^{5}He ground state. The observed width of this peak is approximately 0.7MeV, consistent with known decay parameters [20].

Comparable signatures are seen in the other reaction channels. The $^{9}\text{Be}(^{3}\text{He}, ^{4}\text{He})^{8}\text{Be}$ channel exhibits a sharp peak associated with the exceptionally narrow ground state of ^{8}Be ($\Gamma < 100\,\text{eV}$), while the $^{9}\text{Be}(^{3}\text{He}, ^{7}\text{Li})^{5}\text{Li}$ channel produces a broader feature

with a width near 1.2MeV, in agreement with the established width of the $^{5}\mathrm{Li}_{\mathrm{g.s.}}$ resonance [20].

Of particular interest is the $^{3}\mathrm{He} + {}^{9}\mathrm{Be} \rightarrow {}^{8}\mathrm{Be}^{*} + {}^{4}\mathrm{He} \rightarrow 3\alpha$ channel. In this case, only one α particle is detected, yet its energy distribution reflects the excitation spectrum of the extremely short-lived ^{8}Be nucleus ($\tau \sim 8 \times 10^{-17}$ s) [20]. The data thus reinforce the interpretation that the detected fragments originate from binary decay of unbound nuclei, and in particular that ^{5}He is observed in its ground state as the complementary product to detected ^{7}Be [20].

From the viewpoint of reaction mechanism analysis, the production of ^{5}He may proceed via two alternative pathways: either through direct transfer of a neutron pair from the ^{9}Be nucleus to the ^{3}He projectile, or through emission of an α particle from ^{9}Be , which can be modeled as a loosely bound $^{5}\mathrm{He} + \alpha$ system [16]. To assess the plausibility of ^{5}He formation as a preformed cluster, we also considered the reaction $d + {}^{9}\mathrm{Be} \rightarrow {}^{4}\mathrm{He} + {}^{7}\mathrm{Li}$, in which a similar composite structure resembling an α–triton configuration may play a significant role.

5 The $d(35\ \mathrm{MeV}) + {}^{9}\mathrm{Be}$ Reaction

Energy spectra of detected protons (panel a), deuterons (b), tritons (c), and ^{4}He nuclei (d), produced in the $d(35\ \mathrm{MeV}) + {}^{9}\mathrm{Be}$ reaction [21], are shown in Figure 5. Each spectrum corresponds to a distinct two-body reaction channel: $^{9}\mathrm{Be}(d,p)^{10}\mathrm{Be}$, $^{9}\mathrm{Be}(d,d)^{9}\mathrm{Be}$, $^{9}\mathrm{Be}(d,t)^{8}\mathrm{Be}$, and $^{9}\mathrm{Be}(d,{}^{4}\mathrm{He})^{7}\mathrm{Li}$. As in the previously discussed ^{3}He -induced reactions [18, 19], the spectral shapes reflect the population of excited states in the complementary residual nuclei: ^{10}Be , ^{9}Be , ^{8}Be , and ^{7}Li , respectively.

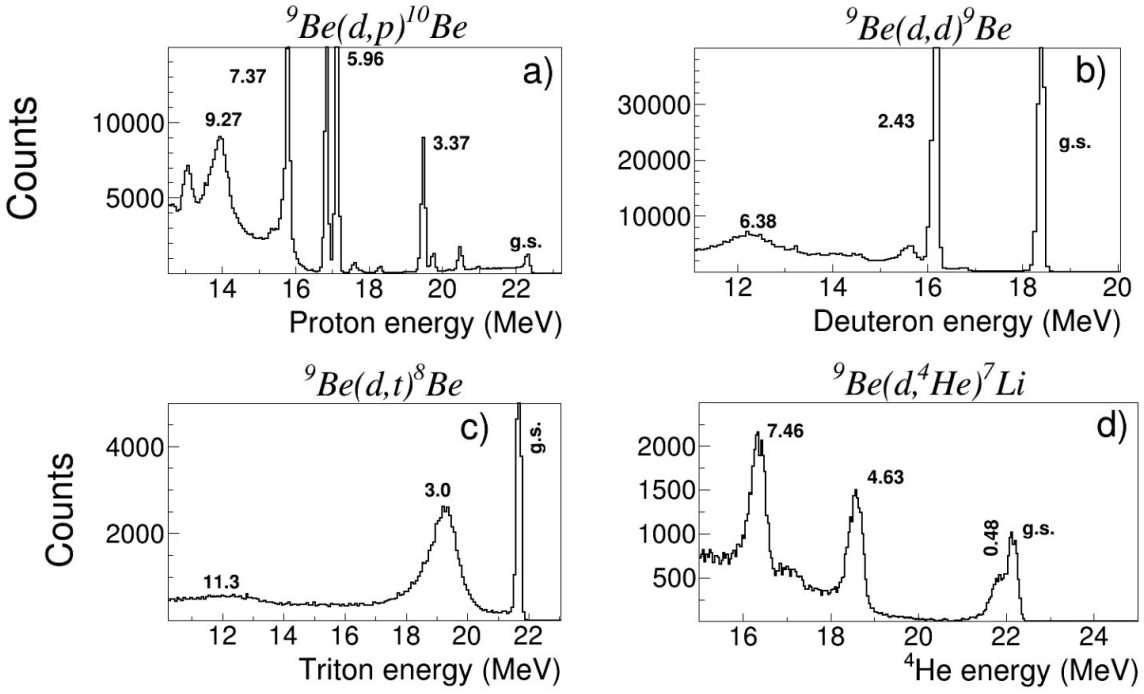

Figure 5: Energy spectra of protons (a), deuterons (b), tritons (c), and ^{4}He (d) measured in the $d(35\ \mathrm{MeV}) + {}^{9}\mathrm{Be}$ reaction [21].

Multiple peaks are observed in each spectrum, corresponding to known excitation

energies. For example, the proton spectrum in panel (a) exhibits prominent peaks at 3.37, 5.96, 7.37, and 9.27 MeV, consistent with discrete levels of ^{10}Be . Similarly, the elastic scattering channel (panel b) reveals clear ground and excited state peaks in ^{9}Be at 0 and 2.43 MeV, as well as a broad structure around 6.38 MeV. In the triton spectrum (panel c), strong population of the ^{8}Be ground state and first excited state at 3.0 MeV is evident, while the ^{4}He spectrum (panel d) shows pronounced peaks corresponding to states in ^{7}Li at 0.48, 4.63, and 7.46 MeV.

These results further support the interpretation of a two-body reaction mechanism, wherein the detected light particles are emitted in coincidence with relatively light residual nuclei. The presence of well-separated, narrow peaks confirms the high resolution of the experimental setup and allows reliable identification of populated nuclear states.

Particularly interesting is the $\mathrm{d} + {}^{9}\mathrm{Be} \rightarrow \alpha + {}^{7}\mathrm{Li}$ channel, which may proceed via two competing mechanisms: direct deuteron pickup or transfer of a ^{5}He cluster from the target nucleus. Although indistinguishable in the final state, these mechanisms exhibit different angular distributions: α particles are emitted preferentially in the forward direction in the pickup scenario, and backward in the cluster-transfer case.

In Ref. [21], we demonstrated that the transfer of a five-nucleon cluster occurs as a single, coherent process rather than a sequence of independent nucleon exchanges [22]. This observation is consistent with previous theoretical and experimental studies, and supports the presence of cluster degrees of freedom in ^{9}Be nucleus.

6 Interaction Time Scale

Among the unbound nuclear systems listed in Table 1, ^{8}Be exhibits the longest lifetime, whereas ^{5}He is the most short-lived. The width of the ^{5}He ground state ($\Gamma = 650$ keV) corresponds to a lifetime of approximately 7×10^{-22} s. This value establishes an upper bound on the timescale over which energy equilibration can occur in reactions where ^{5}He appears as a final-state product. Consequently, the redistribution of energy in light-ion reactions is inferred to proceed on timescales shorter than 10^{-22} s.

Table 1: Properties of selected unbound nuclei [2, 20].

Unstable nucleus	Γ (MeV)	$T_{1/2}$ (s)
^{5}He	0.650	7×10^{-22}
^{6}Be	0.092	5×10^{-21}
^{8}Be	7×10^{-6}	8×10^{-17}
^{9}B	0.540	8×10^{-19}

A general schematic of the time evolution in low-energy heavy-ion collisions is presented in Figure 6, adapted from Ref. [23]. The figure divides the evolution into three characteristic temporal stages. The **first stage** (fast), covering timescales from 10^{-24} to 10^{-22} s, is associated with the initial contact and rapid processes such as **charge** and **momentum equilibration**. The **second stage** (moderate) spans approximately 10^{-22} to 10^{-20} s, during which momentum redistribution continues. Finally, the **third stage** (slow), extending from 10^{-20} up to 10^{-14} s, corresponds to gradual **thermal equilibration** of the system.

Color shading indicates the extent of internal excitation at each stage: orange for early energy deposition, blue for slower thermalization. Arrows above the plot indicate when charge, momentum, and thermal equilibrium are reached. Most internal excitation occurs within the first 10^{-23} s i.e., during initial contact) consistent with prior models.

Our experimental results suggest that equilibration in reactions involving light nuclei such as ^{9}Be occurs on significantly shorter timescales than predicted by the standard model for heavy-ion systems. In particular, the observed spectral structures and widths of unbound nuclei (e.g., ^{5}He and ^{5}Li) imply that full energy equilibration takes place within 10^{-22} s or less [16], highlighting the rapid and direct nature of these cluster-dominated reactions.

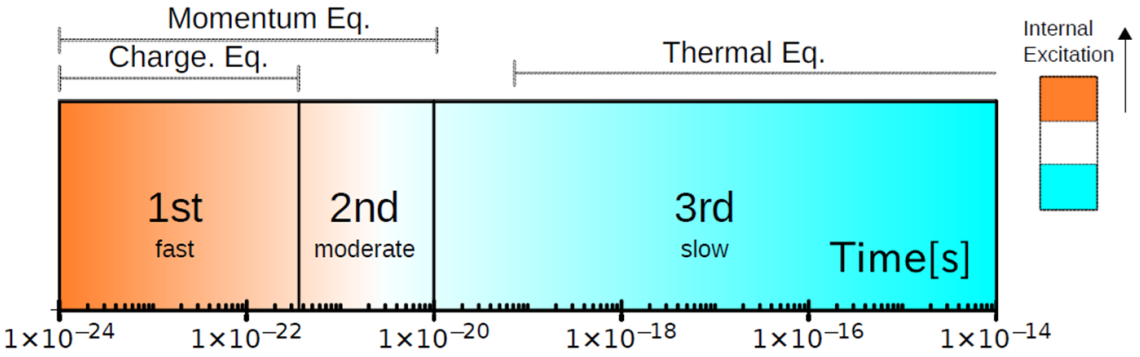

Figure 6: Time evolution of low-energy heavy-ion collisions, showing three characteristic stages: fast (1st), moderate (2nd), and slow (3rd). Charge and momentum equilibrium are achieved rapidly, while full thermalization occurs on longer timescales. Internal excitation is highest at early stages (adapted from Y. Iwata [23]).

Conclusions

Inclusive energy spectra for transfer reactions induced by d, ^{3}He, and ^{4}He projectiles on ^{9}Be have been measured and systematically analyzed. The observed spectral features for outgoing protons, deuterons, tritons, and α particles correspond closely to known excitation levels in complementary nuclei, including ^{10,11,12}B, ^{10}Be, ^{8}Be, ^{7}Li, ^{5}He, and ^{5}Li. The presence of narrow, well-resolved peaks across all studied channels provides strong evidence for two-body reaction mechanisms.

In channels involving unbound nuclear systems, the energy spectra reveal peaks corresponding to ground-state resonances of ^{5}He, ^{5}Li, and ^{8}Be. These results are inconsistent with three-body statistical decay and confirm the population of specific intermediate resonant states. The selective population of such states further supports the role of cluster structure in the entrance and exit channels.

Evidence is presented for the coherent transfer of a ^{5}He cluster, particularly in ^{3}He- and d-induced reactions. The observed correlations and peak shapes are consistent with a direct, single-step cluster-transfer mechanism, as opposed to sequential nucleon exchange.

Finally, time-scale estimates derived from the resonance widths indicate that energy equilibration occurs within $\lesssim 10^{-22}$ s, significantly faster than thermalization times in heavy-ion systems. These findings highlight the prompt, non-statistical

nature of few-body transfer reactions and reinforce the relevance of cluster degrees of freedom in light nuclei.

References

[1] A. T. Rudchik *et al.*, Nucl. Phys. A **609**, 147 (1996).

[2] V. Zagrebaev *et al.*, *DWBA for nucleon transfer reactions*, `http://nrv.jinr.ru/nrv/webnrv/transfer/` (2009), Nuclear Reaction Video Project.

[3] F. C. Young and A. R. Knudson, Nucl. Phys. A **184**, 563 (1972).

[4] C. D è traz *et al.*, Nucl. Phys. A **147**, 488 (1970).

[5] R. M. Devries *et al.*, Phys. Lett. B **32**, 193 (1970).

[6] T. Honda, Y. Kudo, H. Horie, Prog. Theor. Phys. **63**, 872 (1980).

[7] Yu. E. Penionzhkevich *et al.*, J. Phys. G **36**, 025104 (2009).

[8] N. K. Skobelev *et al.*, Phys. Part. Nucl. Lett. **6**, 208 (2009).

[9] T. A. D. Brown *et al.*, Phys. Rev. C **76**, 054605 (2007).

[10] P. Papka *et al.*, Phys. Rev. C **75**, 045803 (2007).

[11] L. V. Grigorenko and M. V. Zhukov, Phys. Rev. C **72**, 015803 (2005).

[12] L. Buchmann *et al.*, Phys. Rev. C **63**, 034303 (2001).

[13] N. Soić *et al.*, Europhys. Lett. **41**, 489 (1998).

[14] R. J. Charity *et al.*, Phys. Rev. C **80**, 024306 (2009).

[15] G. Nyman *et al.*, Nucl. Phys. A **510**, 189 (1990).

[16] S. M. Lukyanov *et al.*, J. Phys. G **41**, 035103 (2014).

[17] C. D è traz *et al.*, Nucl. Phys. A **228**, 39 (1974).

[18] S. Lukyanov *et al.*, World J. Nucl. Sci. Technol. **5**, 265 (2015).

[19] B.A. Urazbekov *et al.*, Chin. Phys. C **48**, 014001 (2024).

[20] NuDat, web application for searching and plotting nuclear structure and decay data, `https://www.nndc.bnl.gov/nudat3/`.

[21] B.A. Urazbekov *et al.*, J. Phys. G: Nucl. Part. Phys. **46**, 105110 (2019).

[22] A. Szczurek, K. Bodek, J. Krug *et al.*, Z. Phys. A **333**, 271 (1989).

[23] Y. Iwata, *J. Phys.: Conf. Ser.* **445**, 012017 (2013).